

# Electroacupuncture treatment improves motor function and neurological outcomes after cerebral ischemia/reperfusion injury

<https://doi.org/10.4103/1673-5374.330617>

Date of submission: April 11, 2021

Date of decision: July 27, 2021

Date of acceptance: September 3, 2021

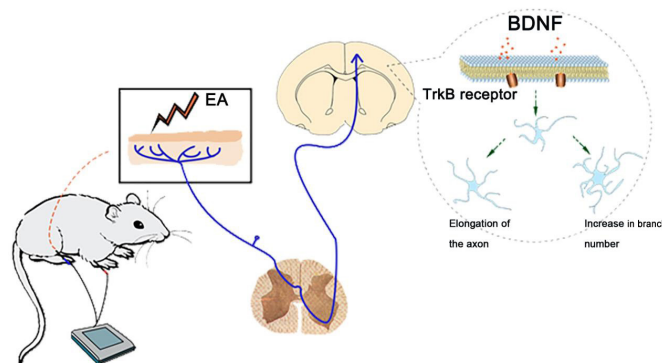
Date of web publication: December 10, 2021

## From the Contents

Introduction	1545
Materials and Methods	1546
Results	1548
Discussion	1553

Si-Si Li<sup>1</sup>, Xu-Yun Hua<sup>2</sup>, Mou-Xiong Zheng<sup>2</sup>, Jia-Jia Wu<sup>3</sup>, Zhen-Zhen Ma<sup>1</sup>, Xiang-Xin Xing<sup>1</sup>, Jie Ma<sup>1</sup>, Chun-Lei Shan<sup>1,3,4</sup>, Jian-Guang Xu<sup>1,4,\*</sup>

**Graphical Abstract** Electroacupuncture (EA) at LI11 and ST36 promotes post-stroke functional recovery in a rat model



## Abstract

Electroacupuncture (EA) has been widely used for functional restoration after stroke. However, its role in post-stroke rehabilitation and the associated regulatory mechanisms remain poorly understood. In this study, we applied EA to the *Zusanli* (ST36) and *Quchi* (LI11) acupoints in rats with middle cerebral artery occlusion and reperfusion. We found that EA effectively increased the expression of brain-derived neurotrophic factor and its receptor tyrosine kinase B, synapsin-1, postsynaptic dense protein 95, and microtubule-associated protein 2 in the ischemic penumbra of rats with middle cerebral artery occlusion and reperfusion. Moreover, EA greatly reduced the expression of myelin-related inhibitors Nogo-A and NgR in the ischemic penumbra. Tyrosine kinase B inhibitor ANA-12 weakened the therapeutic effects of EA. These findings suggest that EA can improve neurological function after middle cerebral artery occlusion and reperfusion, possibly through regulating the activity of the brain-derived neurotrophic factor/tyrosine kinase B signal pathway. All procedures and experiments were approved by the Animal Research Committee of Shanghai University of Traditional Chinese Medicine, China (approval No. PZSHUTCM200110002) on January 10, 2020.

**Key Words:** brain-derived neurotrophic factor; dendritic; electroacupuncture; ischemia/reperfusion; motor function; neurite outgrowth inhibitor-A; neurological outcomes; Nogo receptor; synapse; tyrosine kinase B

Chinese Library Classification No. R454; R743; R245

## Introduction

Cerebral ischemic stroke is caused by cerebral vascular artery stenosis or occlusion, or by insufficient cerebral blood supply (Veltkamp and Gill, 2016; Duris et al., 2018). As the most common type of stroke, ischemic stroke leads to an acute and progressive neurodegenerative condition with high mortality and limited functional recovery (Che et al., 2019). Tissue

damage that is delayed and persistent after ischemic stroke impedes the repair and recovery of brain tissue, causing brain dysfunction (Ali et al., 2018; Kaiser and West, 2020). Neuronal plasticity and tissue repair in the injured brain are important targets for the development of a successful therapy following cerebral ischemic stroke because they influence brain remodeling and subsequent functional recovery

<sup>1</sup>School of Rehabilitation Science, Shanghai University of Traditional Chinese Medicine, Shanghai, China; <sup>2</sup>Department of Traumatology and Orthopedics, Yueyang Hospital of Integrated Traditional Chinese and Western Medicine, Shanghai University of Traditional Chinese Medicine, Shanghai, China; <sup>3</sup>Center of Rehabilitation Medicine, Yueyang Hospital of Integrated Traditional Chinese and Western Medicine, Shanghai University of Traditional Chinese Medicine, Shanghai, China; <sup>4</sup>Engineering Research Center of Traditional Chinese Medicine Intelligent Rehabilitation, Ministry of Education, Shanghai, China

\*Correspondence to: Jian-Guang Xu, PhD, xjg@shutcm.edu.cn.

<https://orcid.org/0000-0003-0601-3403> (Jian-Guang Xu)

**Funding:** This work was supported by the National Key R&D Program of China, No. 2018YFC2001600 (to JGX), the National Natural Science Foundation of China, No. 81902301 (to JJW), Budgetary Project of Shanghai University of Traditional Chinese Medicine of China, No. 2019LK024 (to JJW), Intelligent Medical Program of Shanghai (Municipal) Health Commission of China, No. 2018ZHYL0216 (to CLS), Clinical Science and Technology Innovation Project of Shanghai Shen Kang Hospital Development Center of China, No. SHDC12018126 (to CLS), Accelerated the Development of Traditional Chinese Medicine Three-Year Action Plan Project (of Shanghai Health Commission) of China, Nos. ZY(2018-2020)-CCCX-2001-06 (to JGX and CLS) and ZY(2018-2020)-CCCX-2004-05 (to JGX and CLS).

**How to cite this article:** Li SS, Hua XY, Zheng MX, Wu JJ, Ma ZZ, Xing XX, Ma J, Shan CL, Xu JG (2022) Electroacupuncture treatment improves motor function and neurological outcomes after cerebral ischemia/reperfusion injury. *Neural Regen Res* 17(7):1545-1555.

(Cheatwood et al., 2008; Sakai and Shichita, 2019; Eftimiadi et al., 2021). Alterations in neuroplasticity can involve dendritic atrophy, axonal degeneration, diminished neurogenesis and synaptogenesis, glial cell dysfunction, and decreased levels of neurotrophic factors (Francis and Song, 2011). Neurons in the ischemic core begin to die within minutes after injury, whereas cell death in the peripheral zones of the infarct (the penumbra) occurs over a period of hours to days (Pamenter et al., 2012). Therefore, an important goal of rehabilitation in stroke treatment is to salvage the ischemic penumbra by accelerating neuronal plasticity and facilitating neuronal regeneration.

Neurotrophins are groups of signaling molecules, produced naturally in the brain, that are able to regulate neuronal differentiation and survival, dendritic arborization, synaptic patterning, and axonal projection in the central nervous system (CNS) (Lewin, 1996; Lam et al., 2016). The neurotrophin family includes brain-derived neurotrophic factor (BDNF), nerve growth factor, neurotrophin-3, and neurotrophin-4 (VonDrän et al., 2014). Of these proteins, BDNF is probably the best characterized with respect to its role in neuronal differentiation, survival, and plasticity (Waterhouse and Xu, 2009; Ng et al., 2019). BDNF drives morphological changes such as axonal and dendritic arborization, which can influence dendritic complexity and axon elongation in cortical pyramidal neurons (Sleiman et al., 2016). In addition to its role in neuronal survival and differentiation, BDNF modulates both short- and long-term synaptic transmission (Choo et al., 2017). BDNF acts at both excitatory and inhibitory synapses, and experimental evidence suggests that BDNF may modulate both spontaneous and stimulated neuronal activities (Falcicchia et al., 2018). The physiological actions of BDNF are mediated via the activation of its receptor tyrosine kinase B (TrkB), which is distributed in various types of brain cells, including neurons, microglia, and astrocytes (Ding et al., 2020). The interaction between BDNF and TrkB contributes to the regulation of neurogenesis and neurite outgrowth (Andres-Alonso et al., 2019).

Electroacupuncture (EA), which stems from traditional manual acupuncture, involves the application of electrical currents at specific frequencies to acupoints via electrodes attached to pairs of needles. It is now a widely accepted treatment owing to its superior efficacy, objectivity, and safety (Tian et al., 2016). EA has been applied as a preventative method for various neurological disorders including Alzheimer's disease (Li et al., 2014), ischemic stroke (Liu et al., 2015), and Parkinson's disease (Lei et al., 2016). A functional magnetic resonance imaging study revealed that acupuncture at the *Zusanli* acupoint (ST36) modulates neural activity in the cortex, as well as the limbic and cerebellum areas (Hui et al., 2005). In addition, EA of the ST36 and *Quchi* (LI11) acupoints has been used to treat patients with ischemic stroke in a clinical setting, leading to improvements in stroke-induced dysfunction (Moon et al., 2003; Chen et al., 2020). When a fine needle is inserted into the skin or deeper tissues at the acupoints of the body, sensory receptors are stimulated and signals are transmitted to the CNS via the C-fibers and A $\delta$ -fibers of the peripheral nerves (Xiao et al., 2018). The subsequent response of the CNS involves the modulation of neuroplasticity. However, whether EA at the ST36 and LI11 acupoints improves motor impairment and neurological deficits via regulation of the BDNF/TrkB signaling pathway in the penumbra of rats following ischemia/reperfusion remains unknown.

The aim of this study was to investigate the molecular mechanisms of the beneficial effects of EA at the ST36 and LI11 acupoints in a rat model of middle cerebral artery occlusion and reperfusion (MCAO/R)-induced brain injury. We hypothesized that EA at ST36 and LI11 might ameliorate MCAO/R injury-induced impairments in neurological and motor function by promoting dendritic spine density and synaptic plasticity via the BDNF/TrkB signaling pathway.

## Materials and Methods

### Animals

A total of 141 specific-pathogen-free adult (8-week-old) male Sprague-Dawley rats, weighing between 250 and 270 g, were obtained from the Shanghai Laboratory Animal Center (Shanghai, China; license No. SCXK (Hu) 2017-0012). We did not use female rats because estrogen has been found to mitigate the area of cerebral infarction (Khan et al., 2015). Animal care and all experimental procedures were conducted in accordance with the ethical guidelines of the Animal Research Committee of Shanghai University of Traditional Chinese Medicine, China, which approved the experimental protocol on January 10, 2020 (approval No. PZSHUTCM200110002). All efforts were made to minimize animal suffering. All animals were housed in individual plastic ventilated cages and maintained under standard laboratory conditions (controlled temperature of 23  $\pm$  2°C, 12-hour light/dark cycle). Food and water were provided freely to all rats. All experiments were designed and reported according to the Animal Research: Reporting of *In Vivo* Experiments (ARRIVE) guidelines.

This study was divided into two parts. The goal of the first part was to examine the time course of BDNF expression in a rat model of ischemic penumbra, with the following six time points: 0, 6, and 24 hours, and 3, 5 and 7 days (the time point 0 was considered pre-surgery). The second goal was to clarify the effect of EA treatment in rats with ischemic stroke. The experimental animals were randomly divided into five groups ( $n = 21$ /group): sham, MCAO/R + vehicle (MCAO/R), MCAO/R + EA + vehicle (MCAO/R + EA), MCAO/R + ANA-12 (0.5 mg/kg), and MCAO/R + EA + ANA-12 (0.5 mg/kg) groups.

### MCAO model, drug injection, and neurological evaluation

**Figure 1A** contains a flowchart of the experiment. Rats were anesthetized with an intraperitoneal injection of 30 mg/kg pentobarbital sodium (Shanghai Boyun Biotech, Co., Ltd., Shanghai, China). After making a midline incision at the neck, the left common carotid artery, external carotid artery, and internal carotid artery were exposed. Then, the left internal carotid artery and the common carotid artery distal to the bifurcation were temporarily clamped using microvascular clips. MCAO was performed by gently advancing a nylon monofilament thread with a silicon-coated tip (Jia Ling Biotechnology Co. Ltd., Guangzhou, China) to the origin of the left middle cerebral artery. After 2 hours of MCAO, the monofilament nylon suture was withdrawn to enable the reperfusion process. Rats in the sham group underwent identical surgery, but nylon sutures were not inserted. When a rat rotated to the right while locomoting after MCAO/R surgery, the model was judged to be successful (Liu et al., 2017).

Rats received intraperitoneal injections of either 1 mL normal saline or 0.5 mg/kg ANA-12 (HY-12497, MedChemExpress, Monmouth Junction, NJ, USA) 24 hours after reperfusion and then once per day for 7 consecutive days. ANA-12 was administered 30 minutes prior to EA treatment. The dose of ANA-12 used in the current study was in accordance with that used in previous studies (Wang et al., 2019; Sun et al., 2020).

Neurological deficits were scored in all rats on day 7 after surgery using the Zea Longa scale (Longa et al., 1989) as follows: 0, no neurological deficits; 1, failure to fully extend the right forepaw; 2, circling to the right; 3, falling to the right; and 4, inability to walk spontaneously.

### EA stimulation

In the MCAO/R + EA + vehicle and MCAO/R + EA + ANA-12 groups, the ST36 and LI11 acupoints were subjected to EA stimulation at the right paralyzed limb once a day between 9:00 a.m. and 11:00 a.m. for 7 days, starting 24 hours after MCAO/R surgery. The rats received EA treatment in the awake

state. Specifically, two stainless steel acupuncture needles were inserted into the LI11 (located in the depression lateral to the anterior aspect of the radius joint of the forelimb) and ST36 acupoints (located 5 mm beneath the capitulum fibulae and lateral posterior to the knee joint) (Liu et al., 2016) of the hemiplegic limb at a depth of 2–3 mm (**Figure 1B and C**). A HANS-200E stimulator (Nanjing Jisheng Medical Co., Ltd., Nanjing, China) was used to deliver dilatational wave stimulations at 2/15 Hz. The stimulus intensity was determined as the point at which slight muscle jitters of the limb could be observed, and the treatment lasted for 30 minutes.

### CatWalk gait analysis

To evaluate functional outcomes, we assessed motor function. Specifically, we conducted gait analysis of rats ( $n = 9$ ) from each group using an automated quantitative gait analysis system (CatWalk™, Wageningen, The Netherlands) in accordance with the manufacturer's instructions. The experiment was conducted in a dark and quiet room. Briefly, rats were placed on one side of a runway and allowed to freely cross it. Animals were trained starting 1 week prior to surgery until they were able to make three consecutive uninterrupted runs on the CatWalk runway. Baseline gait analysis was performed for each animal 24 hours prior to surgery, and subsequent measurements were obtained at 1, 3, and 7 days after MCAO/R. CatWalk software 10.6 and CatWalk XT Automatic Footprint Classification software were used to analyze run duration, average run speed, swing speed, stride length, stand time, and body speed.

### 2,3,5-Triphenyltetrazolium chloride staining

Cerebral infarct size was assessed 7 days after reperfusion using 2,3,5-triphenyltetrazolium chloride (TTC; Sigma-Aldrich, St. Louis, MO, USA) staining. The brains were rapidly removed, frozen, and then sliced into five coronal sections (approximately 2 mm apart). Sections were dyed with 2% TTC solution for 20 minutes in the dark at a constant temperature (37°C), and then fixed with 4% paraformaldehyde for at least 1 hour. The infarct size was calculated according to the ratio of the non-TTC-stained area to the TTC-stained area using Image-Pro Plus 6.0 software (Media Cybernetics, Rockville, MD, USA).

### Histology and immunofluorescence

On day 7 after reperfusion, the rats ( $n = 6$ ) were sacrificed following anesthesia, as described above. For the hematoxylin-eosin (H&E) staining, Luxol fast blue (LFB) staining, Nissl staining, terminal deoxynucleotidyl transferase-mediated dUTP-biotin end-labeling (TUNEL) staining, and immunofluorescence analyses, brain tissue samples were fixed with 4% paraformaldehyde and then embedded in paraffin, and 5 μm thick serial sections were prepared and mounted on poly-L-lysine-coated slides. Histopathological examinations were performed using H&E, Nissl, and LFB staining according to the manufacturer's instructions. For the H&E assay (G1003, Servicebio, Wuhan, China), brain sections were prepared and stained with hematoxylin and eosin. Nissl staining was performed with 0.1% Cresyl violet (G1036, Servicebio). An LFB staining kit (G1030, Servicebio) was used to stain myelin tissue and evaluate demyelination. Specifically, the slices were stained with LFB staining solution at 60°C for 1 hour. The slices were then cooled and rinsed with tap water. Subsequently, the slices were differentiated in 70% ethanol and lithium carbonate, and the reaction was terminated with tap water. The degree of differentiation of each section was assessed using a microscope (the myelin appeared blue, whereas the background was nearly colorless). TUNEL was performed using a TUNEL Assay Kit (Cat# G1507, Servicebio). Briefly, the slides were treated with proteinase K for 25 minutes at 37°C. After rinsing them with PBS, the slides were incubated with TUNEL reaction mixture (terminal

deoxynucleotidyl transferase:dUTP:buffer = 1:5:50) for 60 minutes at 37°C. Subsequently, the slides were exposed to diaminobenzidine solution and then stained with hematoxylin solution. For immunofluorescence analysis, dried paraffin-embedded sections were deparaffinized and rehydrated using xylene and graded ethanol. The slides were boiled in 0.01 M sodium citrate buffer (pH 6.0) in a microwave oven for antigen retrieval. Subsequently, the sections were blocked in 3% H<sub>2</sub>O<sub>2</sub> and then incubated in blocking solution (10% normal goat serum with 0.3% Triton X-100) (Solarbio, Beijing, China) at room temperature for 1 hour. The sections were incubated overnight at 4°C with the following primary antibodies diluted in blocking solution: BDNF (1:100, rabbit, Cat# ab108319, RRID: AB\_10862052, Abcam, Cambridge, MA, USA); microtubule-associated protein-2 (MAP-2; 1:200, rabbit, Cat# 17490-1-AP, RRID: AB\_2137880, ProteinTech, Wuhan, China); neurite outgrowth inhibitor A (Nogo-A; 1:100, rabbit, Cat# DF8581, RRID: AB\_2841785, Affinity Biosciences, Cincinnati, OH, USA); and Nogo receptor (NgR; 1:100, rabbit, Cat# DF13593, RRID: AB\_2846612, Affinity Biosciences). After washing the sections with phosphate-buffered saline, they were incubated with Alexa Fluor® 488 AffiniPure goat anti-rabbit IgG (H+L) (1:200, goat, Cat# 33106ES60, RRID: AB\_2338046, Yeasen Biotech, Shanghai, China) for 30 minutes at 37°C. The nuclei were counterstained with 4,6-diamidino-2-phenylindole (Beyotime, Shanghai, China) for 5 minutes. The penumbra area of the ischemic cortex was observed. Images were collected using a fluorescence microscope (Olympus, Tokyo, Japan).

### Western blot analysis

After the experimental period, the ischemic penumbra was carefully removed. Each group contained six rats on day 7 after reperfusion. While on ice, the total protein was extracted from the ischemic penumbra tissue using radio-immunoprecipitation assay buffer with added phenylmethanesulfonyl fluoride (Beyotime) and phosphatase inhibitor (radio-immunoprecipitation assay:phenylmethanesulfonyl fluoride:phosphatase inhibitor = 100:1:2). The total protein concentration was measured using a bicinchoninic acid assay (Beyotime). A total of 80 μg of protein was loaded onto a 10% sodium dodecyl sulfate-polyacrylamide gel electrophoresis gel according to the molecular weight of the target proteins for electrophoresis, and then transferred onto polyvinylidene difluoride membranes (Millipore, Bedford, MA, USA). The membranes were blocked for 1 hour at room temperature with 5% skim milk (Biofrox, Einhausen, Hessen, Germany) in Tris-buffered saline containing 0.1% Tween-20. Then, the membranes of phosphorylated (p)-TrkB were blocked with 5% bovine serum albumin (Solarbio) and probed with specific primary antibodies against BDNF (1:1000, rabbit, Cat# ab108319, RRID: AB\_10862052, Abcam), p-TrkB (1:500, rabbit, Cat# ab229908, RRID: AB\_2892153, Abcam), TrkB (1:500, rabbit, Cat# 4603T, RRID: AB\_2155125, Cell Signaling Technology, Beverly, MA, USA), postsynaptic density protein 95 (PSD95; 1:500, rabbit, Cat# ab18258, RRID: AB\_444362, Abcam), synapsin-1 (1:500, rabbit, Cat# ab8, RRID: AB\_2200097, Abcam), MAP-2 (1:500, rabbit, Cat# 17490-1-AP, RRID: AB\_2137880, ProteinTech), Nogo-A (1:500, rabbit, Cat# DF8581, RRID: AB\_2841785, Affinity Biosciences), NgR (1:500, rabbit, Cat# DF13593, RRID: AB\_2846612, Affinity Biosciences), and β-tubulin (1:1000, rabbit, Cat# 2128S, RRID: AB\_823664, Cell Signaling Technology) overnight at 4°C. After washing, horseradish peroxidase-conjugated goat anti-rabbit IgG (1:5000, goat, Cat# BLO03A, RRID: AB\_2827666, Biosharp, Hefei, China) was added to the membranes, and they were incubated at room temperature for 2 hours. Finally, a chemiluminescence detection kit (Advansta, Menlo Park, CA, USA) was used to visualize the membranes, which were then scanned using an UVP BioSpectrum imaging system (UVP LLC, Upland, CA, USA).

Densitometry analysis of the immunoblots was performed using ImageJ software version 1.8.0 (National Institutes of Health, Bethesda, MD, USA).

### Quantitative real-time polymerase chain reaction

On day 7 after reperfusion, total RNA was extracted from the ischemic penumbra tissue ( $n = 6$  per group) using TRIzol reagent (Invitrogen, Carlsbad, CA, USA). For each sample, complementary DNA was synthesized from 1  $\mu$ g of total RNA using the Reverse Transcription System A3500 (Promega, Madison, WI, USA). Quantitative real-time polymerase chain reactions (qPCR) were performed in triplicate using SYBR Green (Toyobo, Osaka, Japan) on a Roche 480 real-time polymerase chain reaction (PCR) system (Roche, Indianapolis, IN, USA). The thermal cycle parameters were as follows: initial denaturation for 5 minutes at 95°C and 40 cycles of 95°C for 10 seconds, 60°C for 10 seconds, and 72°C for 10 seconds. The tubulin gene was chosen as an internal reference in the qPCR protocol. Relative gene expression was calculated using the  $2^{-\Delta\Delta Ct}$  method (Schmittgen and Livak, 2008). Primer sequences are listed in **Table 1**.

**Table 1 | Primer sequences for quantitative real-time polymerase chain reaction**

Gene	Forward primer (5'–3')	Reverse primer (5'–3')
<i>BDNF</i>	TGT GGT CAG TGG CTG GCT CTC	ACA GGA CGG AAA CAG AAC GAA CAG
<i>Nogo-A</i>	TGC AGT GTT GAT GTG GGT GTT	ATC TGC ACC TGA TGC CGT TC
<i>NgR</i>	TCG GAA GGA GCA GGA CTC AGA AC	TGA GGG AGG CAT AGG ATT GGA CAG
<i>Synapsin-1</i>	GTC CTC ATT CGT GCT GCC TGT G	AGG AGT GGA GGT TGG AGG AAG ATG
<i>PSD95</i>	TCC AGT CTG TGC GAG AGG TAG C	GGA CGG ATG AAG ATG GCG ATG G
<i>Tubulin</i>	CCA GAT GCC AAG CGA CAA GAC C	GGT AGG TGC CAG TGC GAA CTT

BDNF: Brain-derived neurotrophic factor; NgR: Nogo receptor; PSD95: postsynaptic density protein 95.

### Transmission electron microscopy

Three rats from each group were sacrificed on day 7 after reperfusion. Brain tissue samples from the ischemic penumbra region were dissected and fixed for at least 2 hours in glutaraldehyde solution (2.5%) at 4°C. After washing, the samples were fixed in 1% osmic acid and stained with 1% uranyl acetate for 1 and 2 hours, respectively, then dehydrated in gradient acetone solution and embedded in epoxy resin. To locate the areas of interest, semi-thin sections were prepared and stained with toluidine blue. Ultrathin sections of the samples were cut and then observed via transmission electron microscopy (Hitachi, Tokyo, Japan).

### Golgi staining

Tissue samples for Golgi-Cox staining analyses were processed using the FD Rapid GolgiStain Kit (PK401, FD Neurotechnologies, Columbia, MD, USA) according to the manufacturer instructions. Rats ( $n = 3$  per group) were sacrificed on day 7 after reperfusion. Golgi-Cox staining was performed as previously described (Zhang et al., 2018). Briefly, the rat brains (encompassing the approximate region from bregma to +2.0 mm from bregma) (Xie et al., 2019) were first placed in impregnation solution for 2 weeks followed by 3 days in a 30% sucrose solution. Then, they were cut into 150- $\mu$ m coronal sections and stained. Finally, the sections were dehydrated with gradient ethanol and rendered transparent with xylene. The images were viewed under a bright-field microscope (Leica Microsystems, Wetzlar, Germany). The images were quantified using ImageJ software, and Sholl

analysis was conducted using the Fiji Sholl Analysis plugin ([http://fiji.sc/Sholl Analysis](http://fiji.sc/Sholl%20Analysis)). We counted the number of dendrites at 20- $\mu$ m intervals from the soma. We used the NeuronJ plugin in ImageJ software for dendrite branch tracing, and calculated the dendritic length. To determine the density of neuronal dendritic spines, we measured the mean spine density/10  $\mu$ m along the dendrites.

### Statistical analysis

All indicators were analyzed by an independent evaluator. No statistical methods were used to predetermine the sample sizes; however, our sample sizes are similar to those reported in a previous publication (Wang et al., 2021). No animals or data points were excluded from the analysis. Statistical analyses were performed using SPSS 16.0 software (SPSS, Chicago, IL, USA). We used a one-way analysis of variance with least significant difference *post hoc* analysis to evaluate significant differences between groups. All data are represented as the mean  $\pm$  standard deviation (SD), and differences were considered statistically significant when  $P$  values  $< 0.05$ .

## Results

### BDNF expression is decreased in the ischemic penumbra within 7 days after MCAO/R

To assess whether the animal model was successfully established, we first examined the time course of BDNF expression in the rat ischemic penumbra. In our experiment, the levels of BDNF increased early after MCAO/R and peaked at 24 hours, which confirmed that MCAO/R caused injury, followed by a slow decline toward the 7<sup>th</sup> day. Compared with that at hour 0, BDNF expression was lower in the regions containing the ischemic penumbra 7 days after MCAO/R (**Figure 1D**).

### EA improves the recovery of motor and neurological function in rats after MCAO/R

To investigate the effect of EA treatment on motor function in rats after MCAO/R, we conducted gait analyses and compared the MCAO/R + EA and MCAO/R groups. **Figure 2A** contains a schematic diagram of the CatWalk behavioral test. After the model had been established, the run duration was prolonged ( $P < 0.01$ ) and the run average speed had decreased ( $P < 0.01$ ). After EA treatment, the run duration decreased ( $P < 0.05$ ), indicating an increase in the run average speed ( $P < 0.01$ ; **Figure 2B** and **C**). EA also improved the body speed ( $P < 0.05$ ; **Figure 2D** and **E**). The stand time of the right limbs was severely affected in animals subjected to surgery, and there was no significant difference in stand time for the right forelimb between the MCAO/R and MCAO/R + EA groups (**Figure 2F**). EA treatment contributed only to the recovery of function in the right hindlimb ( $P < 0.05$ ; **Figure 2G**). The swing speed results were in agreement with the stand time results ( $P < 0.05$ ; **Figure 2H** and **I**). Stride length was significantly decreased in the MCAO/R group relative to the sham group ( $P < 0.01$ ). Nevertheless, the stride length of the right limbs had significantly increased after 7 days of EA administration ( $P < 0.05$ ; **Figure 2J** and **K**).

We used neurological deficit scores in the present study to examine the neuroprotective effect of EA treatment. In the sham group, no rats displayed symptoms of neurological deficits, whereas there were outstanding neurological deficits in the MCAO/R group. EA treatments significantly reduced the occurrence of neurological deficits in the MCAO/R + EA compared with the MCAO/R group ( $P < 0.05$ ). Furthermore, intervention with ANA-12 clearly weakened the effect of EA treatments compared with the MCAO/R + EA group ( $P < 0.01$ ; **Figure 3A**).

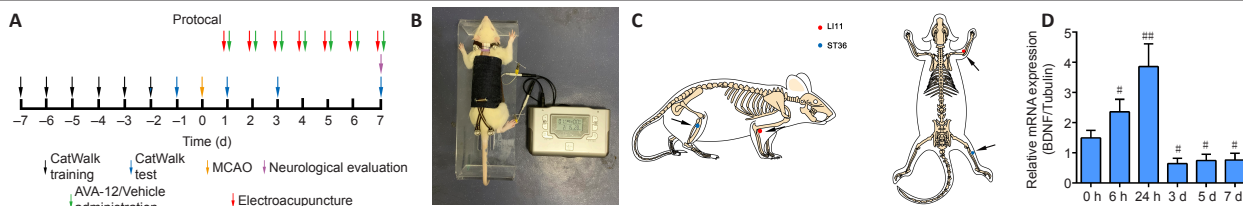


**Figure 1 | Time course of BDNF expression in the cortical ischemic penumbra and experimental protocol.** (A) Flowchart of the experiment. (B) Rat that received EA treatment in the awake state. (C) The locations of the *Quchi* (LI11) and *Zusanli* (ST36) acupoints. (D) The mRNA expression of BDNF in the ischemic penumbra cortex was measured using quantitative real-time polymerase chain reactions. Data are presented as the mean  $\pm$  SD ( $n = 6$ ).  $\#P < 0.05$ ,  $\#\#\#P < 0.01$ , vs. sham group (one-way analysis of variance followed by least significant difference *post hoc* test). The experiments were repeated three times. BDNF: Brain-derived neurotrophic factor; EA: electroacupuncture; MCAO: middle cerebral artery occlusion.

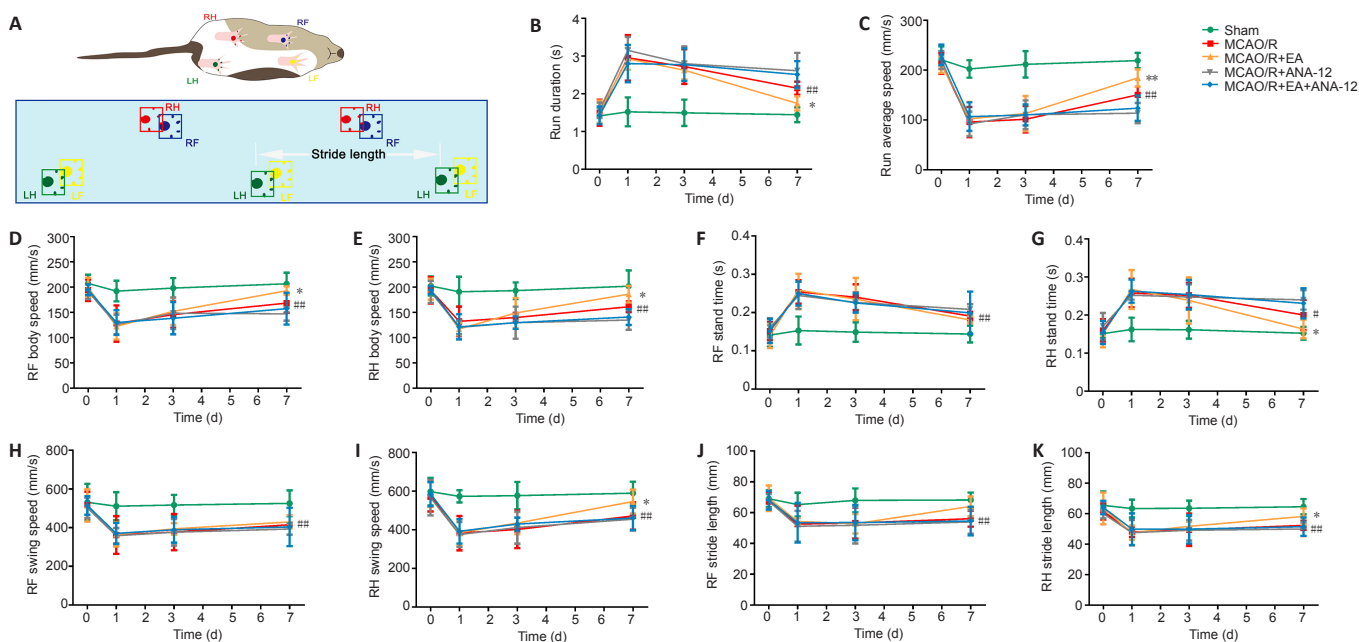


**Figure 2 | EA improves functional recovery after ischemic stroke in terms of gait.** EA treatment was applied at the LI11 and ST36 acupoints in MCAO/R rats. ANA-12 was administered via intraperitoneal injection at 0.5 mg/kg once per day for 7 consecutive days. (A) Schematic of the CatWalk behavioral test. (B) Run duration. (C) Run average speed. (D, E) RF and RH body speed. (F, G) RF and RH stand time. (H, I) RF and RH swing speed. (J, K) RF and RH stride length. Data are presented as the mean  $\pm$  SD ( $n = 9$ ).  $\#P < 0.05$ ,  $\#\#\#P < 0.01$ , vs. sham group;  $*P < 0.05$  vs. MCAO/R group (one-way analysis of variance followed by least significant difference *post hoc* test). The experiments were repeated three times. ANA-12: TrkB inhibitor; EA: electroacupuncture; LF: left forelimb; LH: left hindlimb; MCAO: middle cerebral artery occlusion and reperfusion; RF: right forelimb; RH: right hindlimb; TrkB: tyrosine kinase B.

### EA attenuates brain damage and neuronal apoptosis in MCAO/R rats

TTC staining revealed no infarctions in the sham group. The sizes of the infarct regions were different in each MCAO/R group. Cerebral infarction was detected in the MCAO/R group, and the infarct volume was significantly increased compared with that in the sham group ( $P < 0.01$ ). Following the EA intervention, the area of the cerebral infarction significantly decreased compared with the MCAO/R group ( $P < 0.05$ ). Furthermore, ANA-12 attenuated the effect of EA treatments ( $P < 0.01$ ; **Figure 3B** and **C**). H&E staining indicated that there were no obvious pathological changes in the ischemic penumbra of the sham group; the structure of the tissue was normal, the cells were arranged in an organized manner, and the intercellular space was dense with no edema. Different degrees of vacuolar necrosis, enlarged interspaces, interstitial edema, and shrinking cell nuclei with deep staining were observed in the MCAO/R group (**Figure 3D**). Additionally, as shown in **Figure 3E**, the results of Nissl staining demonstrated that the number of pyknotic and fragmented neurons had increased in the MCAO/R group, and the Nissl bodies exhibited signs of dissolution and necrosis. Some deformed and necrotic cells were present in the EA group. The condition of the tissue in the MCAO/R + ANA-12 group was worse than that in the other groups.

### EA enhances the activation of the BDNF/TrkB signaling pathway in the ischemic penumbra of MCAO/R rats

In the present study, we investigated whether the administration of EA affected the expression of BDNF, TrkB, and p-TrkB in the ischemic penumbra after MCAO/R. As shown in **Figure 4A**, immunofluorescence staining indicated a clear decrease in BDNF immunopositivity in the MCAO/R group compared with the sham group ( $P < 0.01$ ), whereas there was a marked increase in BDNF levels in the EA group compared with the MCAO/R group ( $P < 0.01$ ). Western blot analysis revealed a significant reduction in BDNF and p-TrkB expression after modeling compared with the sham group ( $P < 0.01$ ). Although the administration of ANA-12 did not modify the expression levels of BDNF compared with the MCAO/R group ( $P > 0.05$ ), the neuroprotective effect of EA on proteins downstream from BDNF was significantly blocked by ANA-12. The protein level of p-TrkB was greatly increased by EA compared with the MCAO/R group ( $P < 0.01$ ), but was notably decreased by ANA-12 administration compared with the MCAO/R + EA group ( $P < 0.01$ ). There was no significant difference in TrkB expression between the groups ( $P > 0.05$ ; **Figure 4B–D**). The qPCR results revealed an obvious increase in BDNF mRNA levels after EA treatment compared with the MCAO/R group ( $P < 0.05$ ; **Figure 4E**).

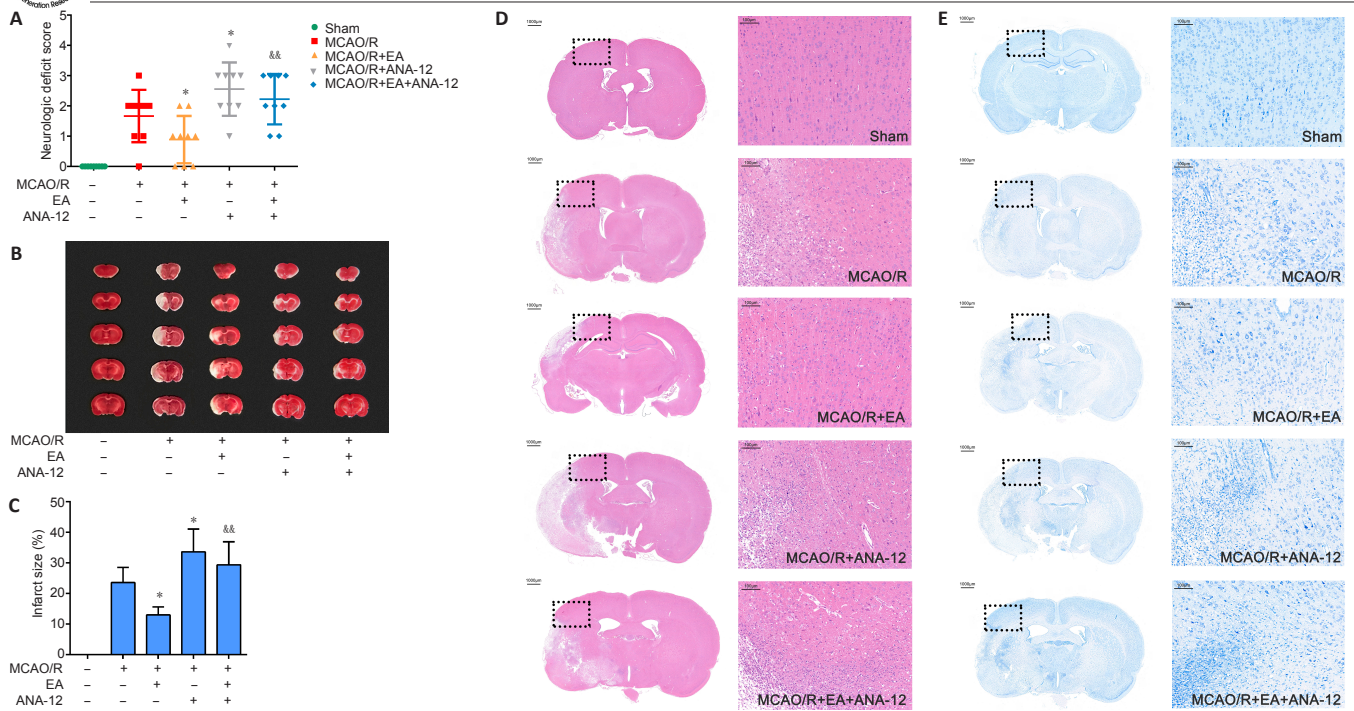


**Figure 3 | Effects of EA on MCAO/R-induced brain injury in rats at 7 days after MCAO/R.** EA was applied at the LI11 and ST36 acupoints in MCAO/R-treated rats. ANA-12 was delivered via intraperitoneal injection at 0.5 mg/kg once per day for 7 consecutive days. (A) Effect of EA on neurologic deficit scores 7 days after MCAO/R according to the Zea Longa score ( $n = 9$ ). (B) 2,3,5-Triphenyltetrazolium chloride staining of brain slices. Normal tissue is shown in red and infarcted tissue in white. The infarct volume in the MCAO/R group was significantly increased compared with that in the sham group, the area of the cerebral infarction was significantly decreased after EA compared with that in the MCAO/R group, and ANA-12 attenuated the effect of EA treatments. (C) Quantitative analyses of infarct size ( $n = 6$ ). Data are presented as the mean  $\pm$  SD.  $\#P < 0.05$ ,  $\#\#\#P < 0.01$ , vs. sham group;  $*P < 0.05$ , vs. MCAO/R group;  $\&\&P < 0.01$ , vs. MCAO/R + EA group (one-way analysis of variance followed by least significant difference *post hoc* test). (D, E) Representative hematoxylin-eosin and Nissl staining performed on sections from ischemic brains ( $n = 6$ ). The ischemic penumbra histopathological alterations and neuronal loss induced by the MCAO/R were alleviated after treatment with EA. Scale bar: 1000  $\mu$ m (left) and 100  $\mu$ m (right). The experiments were repeated three times. ANA-12: TrkB inhibitor; EA: electroacupuncture; MCAO/R: middle cerebral artery occlusion and reperfusion; TrkB: tyrosine kinase B.

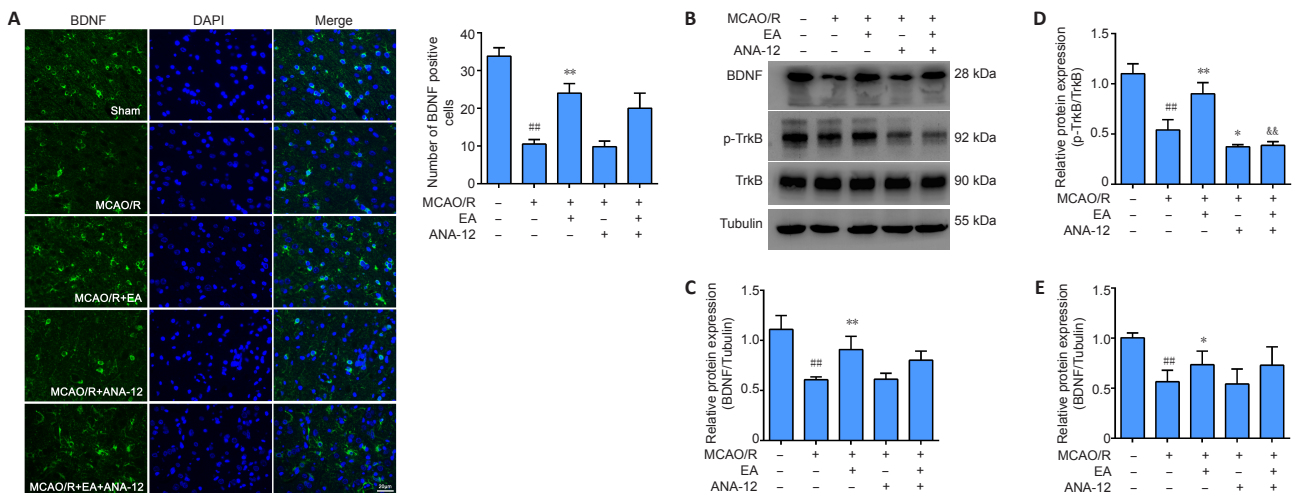


**Figure 4 | EA increases the expression of BDNF and p-TrkB in the cortical ischemic penumbra 7 days after MCAO/R.** EA treatment was performed at the LI11 and ST36 acupoints in MCAO/R-treated rats. ANA-12 was delivered by intraperitoneal injection at 0.5 mg/kg once per day for 7 consecutive days. (A) Representative immunofluorescence images indicating BDNF-positive expression (green, Alexa Fluor 488). Blue: DAPI. BDNF expression in the MCAO/R group was decreased compared with that in the sham group, whereas the expression of BDNF in the EA-treated group was dramatically higher than that in the MCAO/R group. Scale bar: 20  $\mu$ m. (B–D) BDNF and p-TrkB protein expression in the cortical ischemic penumbra determined by western blot analysis. (E) BDNF mRNA expression in the ischemic penumbra was detected by quantitative real-time polymerase chain reaction. Data are presented as the mean  $\pm$  SD ( $n = 6$ ).  $\#\#\#P < 0.01$ , vs. sham group;  $*P < 0.05$ ,  $**P < 0.01$ , vs. MCAO/R group;  $\&\&P < 0.01$ , vs. MCAO/R + EA group (one-way analysis of variance followed by least significant difference *post hoc* test). The experiments were repeated three times. ANA-12: TrkB inhibitor; BDNF: brain-derived neurotrophic factor; DAPI: 4,6-diamidino-2-phenylindole; EA: electroacupuncture; MCAO/R: middle cerebral artery occlusion and reperfusion; p-TrkB: phosphorylated-tyrosine kinase B; TrkB: tyrosine kinase B.

**EA inhibits MCAO/R-induced activation of Nogo-A and NgR and promotes myelin repair in the ischemic penumbra**

To evaluate the beneficial effect of EA on myelin repair, we performed specific staining using LFB, which is used as a highly sensitive marker of myelin loss, to determine overall

myelination (Qin et al., 2018). Although LFB staining showed no evidence of demyelination in the sham group, there was a loss of myelin in destructive lesions post-MCAO/R, and the outcome in the MCAO/R + ANA-12 group was worse than that in the MCAO/R group. Demyelination was significantly

reduced in EA-treated rats compared with the MCAO/R group (Figure 5A). Next, we evaluated the expression of Nogo-A and NgR in each group. The immunofluorescence staining suggested that MCAO/R increased the positive expression of Nogo-A and NgR in the ischemic penumbra compared with the sham group (Figure 5B and C). The protein level of Nogo-A in brain tissue was significantly increased in the MCAO/R group compared with the sham group ( $P < 0.01$ ), and the changes in expression could be reversed by EA treatment ( $P < 0.01$ ). NgR protein levels in the EA group followed the same trend as the Nogo-A levels ( $P < 0.05$ ; Figure 5D–F). The same tendency was observed for the mRNA expression levels of Nogo-A and NgR, as determined by qPCR analysis (Figure 5G and H).

### EA promotes dendritic growth through the BDNF/TrkB signaling pathway in the ischemic penumbra of MCAO/R rats

Figure 6A–C shows representative coronal Golgi-Cox staining illustrating the phenomenon of MCAO/R injury, and the demarcation between the apical and basal dendrites is illustrated in Figure 6D. To investigate changes in dendritic complexity and the mechanism by which EA promotes dendritic growth, we performed Sholl analysis in which we counted the number of intersections along the dendritic trees at all distances from the soma in terms of concentric circles separated by 20  $\mu\text{m}$  (Figure 6E and F). Sholl analysis revealed a significant reduction in the number of intersections along the apical and basal dendrites after ischemia/reperfusion injury compared with the sham group ( $P < 0.01$ ) (Figure 6G and H). In addition, we found marked and highly significant reductions in dendrite branches in both apical ( $P < 0.05$ ) and basal ( $P < 0.01$ ) regions in the MCAO/R group compared with the sham group (Figure 6I and J), with notable reductions in the total lengths of branches (apical branches:  $P < 0.01$ ; basal branches  $P < 0.05$ ; Figure 6K and L). Nevertheless, EA effectively rescued the damage to dendrite structure caused by MCAO/R and facilitated regrowth after injury. The dendritic growth was poorest in the MCAO/R + ANA-12 group.

### EA promotes dendritic spine density and synaptic plasticity through the BDNF/TrkB signaling pathway in the ischemic penumbra of MCAO/R rats

We observed the ultrastructure of the synapses using an electron microscope. Transmission electron microscopy showed that the synapses in the sham group were well preserved, and examination of the synaptic ultrastructure of ischemic penumbra neurons revealed a reduced number of synaptic vesicles after surgery. The synaptic structure in the MCAO/R + EA group was markedly improved after treatment, with thickened synaptic membranes and more synaptic vesicles, as well as tighter synaptic connections. The MCAO/R + ANA-12 group had the poorest performance among the groups (Figure 7A). The generation, maturation, and long-term stabilization of dendritic spines contribute to experience-dependent synaptic plasticity (Padmanabhan et al., 2019). We next determined whether EA affected the plasticity of dendritic spines. The results showed that the densities in both the apical ( $P < 0.05$ ) and basal ( $P < 0.01$ ) dendritic spines were markedly decreased in MCAO/R rats compared with the sham group, and that this was dramatically rescued by administration of EA (apical dendritic spines:  $P < 0.05$ , basal dendritic spines:  $P < 0.01$ ; Figure 7B–E). We then investigated the role of EA treatment in synaptic plasticity by evaluating changes in synaptic proteins. EA treatment followed by MCAO/R resulted in significant increases in both the mRNA and protein levels of PSD95 (mRNA:  $P < 0.01$ ; protein:  $P < 0.05$ ) and synapsin-1 (mRNA:  $P < 0.05$ ; protein:  $P < 0.01$ ) compared with the MCAO/R group ( $P < 0.05$  or  $P < 0.01$ ; Figure 7F–J), as well as levels of MAP-2 ( $P < 0.05$ ; Figure 8A–C). We used a TUNEL assay to examine whether the protective effect of EA was associated with a reduction in apoptosis. The results indicated that the number of apoptotic cells had increased post-MCAO/R, and that EA-treated rats had few apoptotic cells compared with the MCAO/R group ( $P < 0.05$ ). ANA-12 significantly increased the number of apoptotic cells compared with the MCAO/R + EA group ( $P < 0.01$ ; Figure 8D).

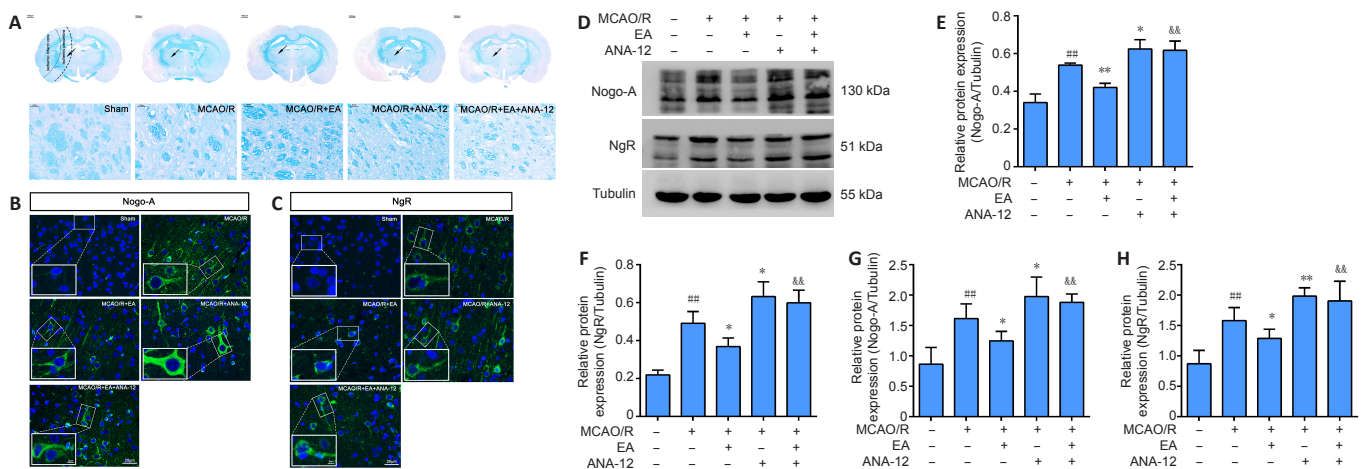


**Figure 5 | EA promotes the repair of myelin in the ischemic penumbra and inhibits the expression of Nogo-A and NgR 7 days after MCAO/R.**

EA treatment was performed at the LI11 and ST36 acupoints in MCAO/R rats. ANA-12 was delivered via intraperitoneal injection at 0.5 mg/kg once per day for 7 consecutive days. (A) Representative images of Luxol fast blue staining at 7 days. There was a loss of myelin in destructive lesions post-MCAO/R, demyelination was significantly reduced after EA intervention, and the outcome in the MCAO/R + ANA-12 group was worse than that in the MCAO/R group. The arrow indicates the myelin in the ischemic penumbra. Scale bars: 1000  $\mu\text{m}$  (upper) and 50  $\mu\text{m}$  (lower). (B) Representative immunofluorescence images of Nogo-A (green, Alexa Fluor 488) in the ischemic penumbra. Nogo-A was significantly increased in the MCAO/R group compared with the sham group, and it could be reversed by EA treatment. Green: Nogo-A; blue: DAPI. Scale bars: 20  $\mu\text{m}$  and 5  $\mu\text{m}$  in the enlarged part. (C) The results of the immunofluorescence examination of NgR (green, Alexa Fluor 488) in the ischemic penumbra. Blue: DAPI. NgR expression was increased in the MCAO/R group, and significantly decreased after the EA intervention. Scale bars: 20  $\mu\text{m}$  and 5  $\mu\text{m}$  in the enlarged part. (D–H) EA inhibited the MCAO/R-induced protein expression of Nogo-A and NgR in the ischemic penumbra cortex, as determined by western blot. (G, H) Nogo-A and NgR mRNA expression levels were detected via quantitative real-time polymerase chain reaction. Data are presented as the mean  $\pm$  SD ( $n = 6$ ). ### $P < 0.01$ , vs. sham group; \* $P < 0.05$ , \*\* $P < 0.01$ , vs. MCAO/R group; && $P < 0.01$ , vs. MCAO/R + EA group (one-way analysis of variance followed by least significant difference *post hoc* test). The experiments were repeated 3 times. ANA-12: TrkB inhibitor; DAPI: 4,6-diamidino-2-phenylindole; EA: electroacupuncture; MCAO/R: middle cerebral artery occlusion and reperfusion; NgR: Nogo receptor; TrkB: tyrosine kinase B.

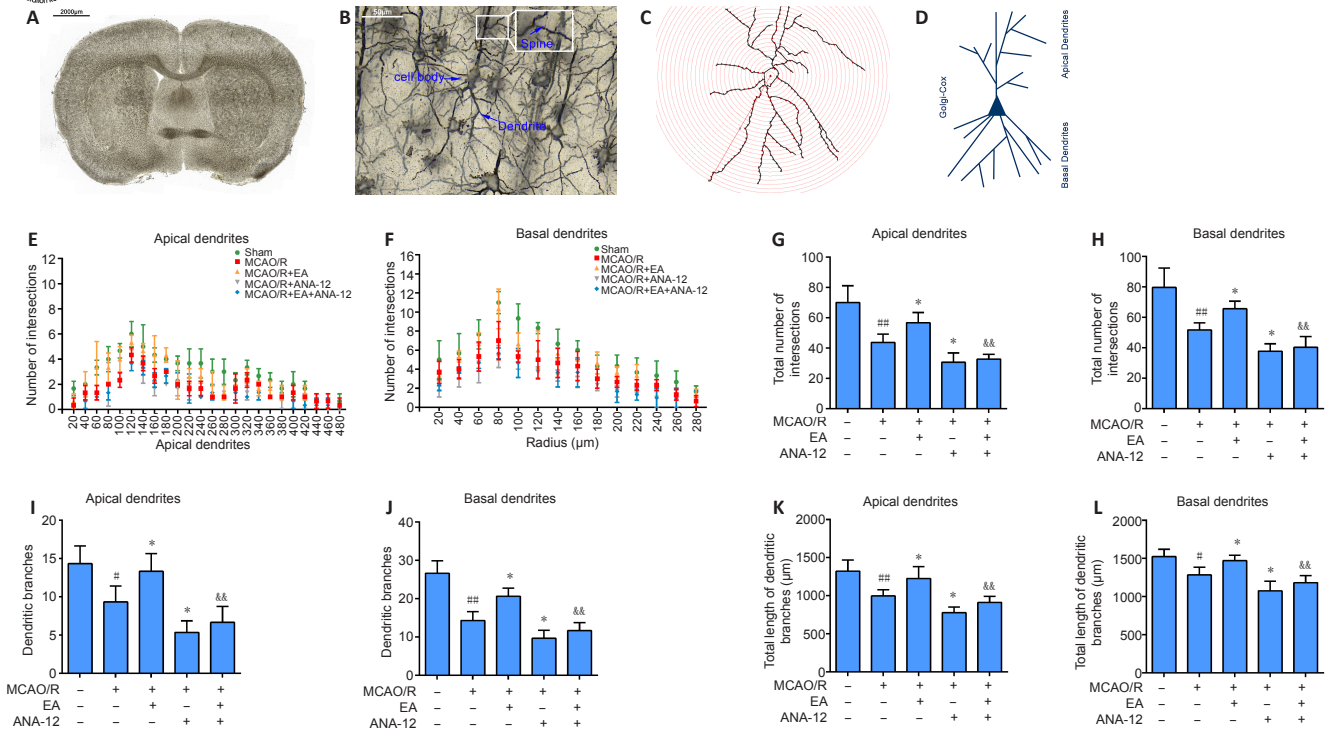


**Figure 6 | EA promotes dendritic branching and growth in the ischemic penumbra.**

EA treatment was performed at the LI11 and ST36 acupoints in MCAO/R rats. ANA-12 was delivered via intraperitoneal injection at 0.5 mg/kg once per day for 7 consecutive days. (A–C) A representative coronal Golgi-Cox staining section illustrating the phenomenon of MCAO/R injury. Scale bars: 2000 µm in A and 50 µm in B. (D) Illustration of the demarcation between the apical and basal dendrites. (E, F) Sholl analysis of the complexity of the dendritic arborization of neurons, represented as dendritic intersections at a given distance from the soma. (G, H) Total number of apical (G) and basal (H) intersections. (I, J) Number of apical (I) and basal (J) dendritic branches. (K, L) Quantification of total apical (K) and basal (L) dendritic length. Data are presented as the mean ± SD ( $n = 3$ ). # $P < 0.05$ , ## $P < 0.01$ , vs. sham group; \* $P < 0.05$ , vs. MCAO/R group; && $P < 0.01$ , vs. MCAO/R + EA group (one-way analysis of variance followed by least significant difference *post hoc* test). The experiments were repeated three times. ANA-12: TrkB inhibitor; EA: electroacupuncture; MCAO/R: middle cerebral artery occlusion and reperfusion; TrkB: tyrosine kinase B.

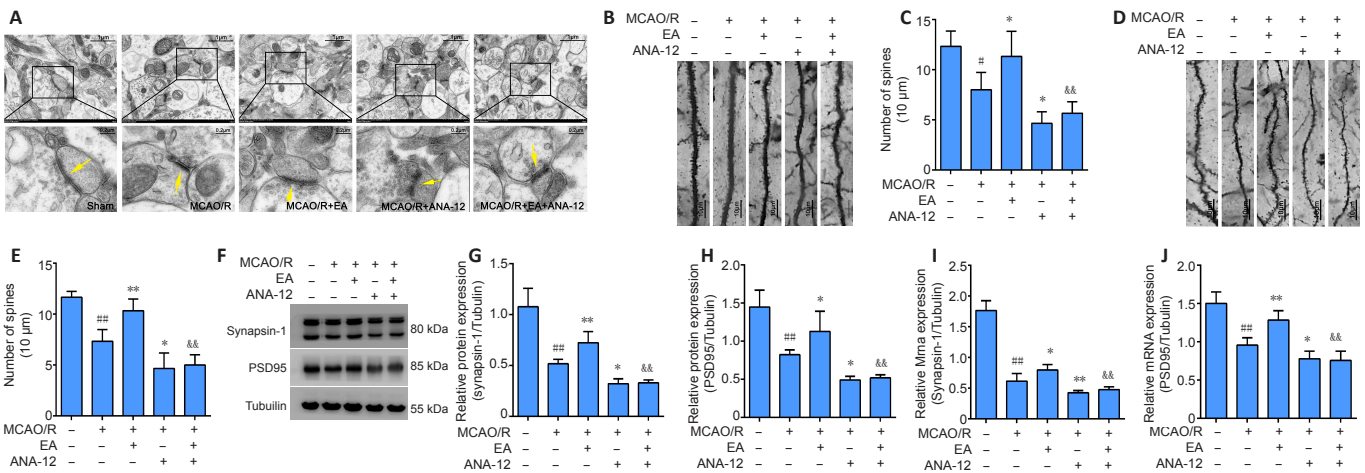


**Figure 7 | EA reverses impaired spine density and increased levels of synaptic-related proteins in the ischemic penumbra.**

EA treatment was performed at the LI11 and ST36 acupoints in MCAO/R rats. ANA-12 was delivered via intraperitoneal injection at 0.5 mg/kg once per day for 7 consecutive days. (A) Representative electron microscopy images of the synaptic structures ( $n = 3$ ). The synaptic ultrastructure revealed a reduced number of synaptic vesicles in the MCAO/R group, markedly improved synaptic structure in the MCAO/R + EA group, and relatively poor performance in the MCAO/R + ANA-12 group. The arrows indicate synapses. Scale bars: 1 µm (upper) and 0.2 µm (lower). (B, C) Density of apical dendritic spines. The densities in the apical dendritic spines were markedly decreased in MCAO/R rats compared with the sham group, and this was dramatically rescued by the administration of EA. Scale bars: 10 µm. (D, E) Density of basal dendritic spines. The densities in the basal dendritic spines were markedly decreased in MCAO/R rats compared with the sham group, and this was dramatically rescued by administration of EA. Scale bars: 10 µm. (F–H) EA increased the protein expression of synapsin-1 and PSD95 in the ischemic penumbra cortex, as determined by western blot. (I, J) Synapsin-1 and PSD95 mRNA expression levels were assessed by quantitative real-time polymerase chain reaction. Data are presented as the mean ± SD ( $n = 6$ ). ## $P < 0.01$ , vs. sham group; \* $P < 0.05$ , \*\* $P < 0.01$ , vs. MCAO/R group; && $P < 0.01$ , vs. MCAO/R + EA group (one-way analysis of variance followed by least significant difference *post hoc* test). The experiments were repeated three times. ANA-12: TrkB inhibitor; EA: electroacupuncture; MCAO/R: middle cerebral artery occlusion and reperfusion; PSD95: postsynaptic density protein 95; TrkB: tyrosine kinase B.

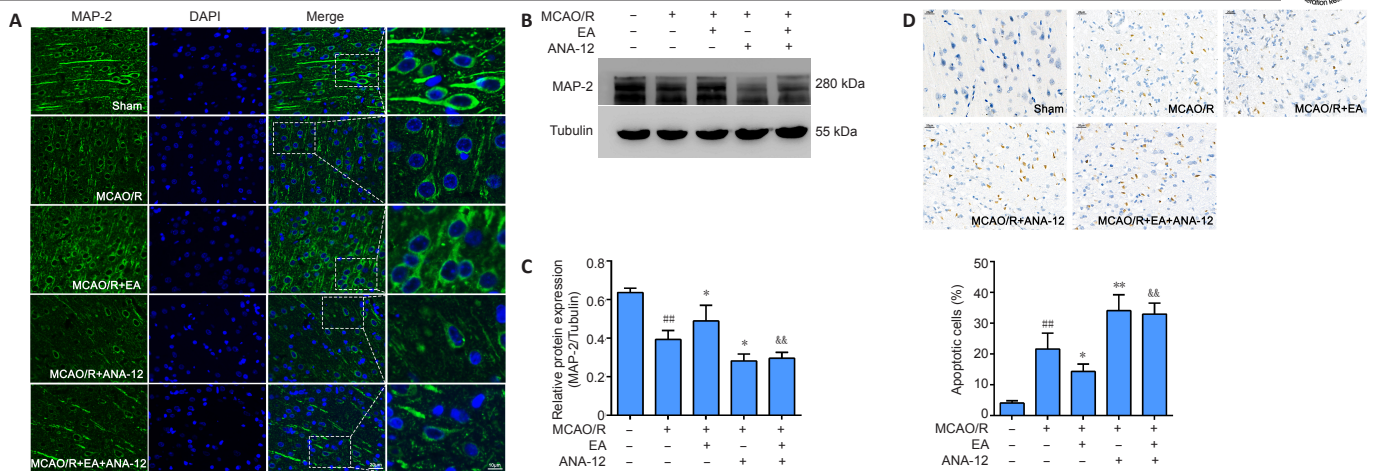


**Figure 8 | EA promotes the expression of MAP-2 and reduces injury-induced neuronal apoptosis in the ischemic penumbra area.** EA treatment was performed at the LI11 and ST36 acupoints in MCAO/R rats. ANA-12 was delivered via intraperitoneal injection at 0.5 mg/kg once per day for 7 consecutive days. (A) Representative immunofluorescence images indicating MAP-2 immunopositivity (green, Alexa Fluor 488). Blue: DAPI. MAP-2 expression was significantly increased in the MCAO/R + EA group compared with the MCAO/R group. Scale bars: 20  $\mu$ m (left three columns) and 10  $\mu$ m (right most column). (B, C) EA promoted the expression of MAP-2 in the ischemic penumbra, as determined by western blot. (D) Apoptosis in the rat ischemic penumbra cortex in each group was measured by TUNEL. The number of apoptotic cells was increased post-MCAO/R, and EA-treated rats had few apoptotic cells compared with the MCAO/R group. Scale bars: 20  $\mu$ m. Data are presented as the mean  $\pm$  SD ( $n = 6$ ). <sup>###</sup> $P < 0.01$ , vs. sham group; <sup>\*</sup> $P < 0.05$ , <sup>\*\*</sup> $P < 0.01$ , vs. MCAO/R group; <sup>&&</sup> $P < 0.01$ , vs. MCAO/R + EA group (one-way analysis of variance followed by least significant difference *post hoc* test). The experiments were repeated three times. ANA-12: TrkB inhibitor; DAPI: 4,6-diamidino-2-phenylindole; EA: electroacupuncture; MAP-2: microtubule-associated protein 2; MCAO/R: middle cerebral artery occlusion and reperfusion; TrkB: tyrosine kinase B; TUNEL: terminal deoxynucleotidyl transferase-mediated dUTP-biotin end-labeling.

## Discussion

Cerebral ischemic stroke induces a series of pathological changes in local brain tissue, and the regeneration of this tissue is essential for functional recovery following stroke. Several previous studies have demonstrated that BDNF may participate in reparative processes after ischemic stroke (Wang et al., 2004; Qin et al., 2014). However, whether EA at the ST36 and LI11 acupoints promotes motor function and neurological recovery via regulation of the BDNF/TrkB signaling pathway in the penumbra of rats remains unclear. In the present study, we established a rat model of MCAO/R to imitate the pathogenesis of ischemic stroke. To our knowledge, this is the first study to use TrkB-specific inhibitors to reveal that EA at the ST36 and LI11 acupoints can have a neuroprotective effect in rats following cerebral ischemia/reperfusion injury, and to demonstrate that EA treatment can recover motor function through modulation of the BDNF/TrkB pathway.

EA has been shown to reduce neuronal apoptosis and promote neurobehavioral recovery in rats following ischemic stroke by increasing irisin levels in the blood and perilesional cortex (Liu et al., 2021). Previous studies have demonstrated that EA can effectively reduce the area of a cerebral infarction and improve modified neurologic severity scores, such that motor scores have been significantly correlated with the functional connectivity of the primary motor cortex in the bilateral hemispheres after cerebral infarction (Li et al., 2021; Liu et al., 2021). However, the precise mechanisms of the neuroprotective effect of EA on ischemic stroke are still not fully understood. Acupoints are specific locations on the body surface where the *qi* and blood (*qi* and blood are the most basic substances that constitute the human body and maintain life according to TCM theory) flow corresponding to meridians and *Zang-fu* organs (*Zang-fu* mainly refers to internal organs of the body) intersect (Xu et al., 2020). Acupoint specificity refers to the difference in indicative range and curative efficacy between real acupoints and non-acupoints. This is an important theoretical basis for acupoint selection, and involves the specificity of clinical efficacy and biological response (Zhao et al., 2012). Acupuncture at acupoints has been found to significantly reduce injury volume compared with acupuncture applied to non-acupoints, which had no clear effects on injury

volume. Moreover, acupuncture at acupoints has been found to play an important role in improving metabolic recovery after stroke (Liu et al., 2013). Based on the meridian theory of traditional Chinese medicine, “Treating Flaccid Paralysis by *Yangming* Alone” is one of the most commonly used rehabilitation methods in the treatment of stroke, and is currently used in clinical settings (Zou et al., 2020). Thus, the acupoints used in this study were functionally related to motor dysfunction after stroke. LI11 and ST36 are sea points of the *Yangming* large intestine meridian of the hand and *Yangming* stomach meridian of the foot, and are frequently used in the clinical management of stroke in China (Liu et al., 2016). EA stimulation at LI11 and ST36 can influence neurogenesis, cell proliferation, and anti-apoptosis in rats following ischemic stroke (Chavez et al., 2017). A previous study demonstrated that acupuncture in human patients following ischemic stroke led to a relative improvement in hemiplegic gait cycle, stand time, and swing time (Zheng et al., 2014). In the current study, CatWalk gait analysis demonstrated that gait parameters such as body speed, stand time, swing speed, and stride length improved after EA treatment. Although the ability of EA treatment to recover MCAO/R-induced functional deficits in some single gait parameters did not reach statistical significance, we observed a beneficial trend compared with the MCAO/R group. However, the treatment efficacy of EA was hampered by the application of ANA-12. H&E and Nissl staining showed that the EA treatment significantly alleviated neuronal injury. Moreover, TTC staining revealed that EA treatment significantly reduced the cerebral infarct volume, which indicates that EA can decrease cell death in the area of the ischemic penumbra. Our findings regarding neurological deficits and CatWalk gait analyses showed that EA treatment significantly improved the recovery of motor function in the limbs of rats post-MCAO/R.

BDNF plays a key role in regulating synaptic plasticity by enhancing neuronal protein synthesis (Bathina and Das, 2015), and TrkB is crucial to neuronal survival and structural plasticity (Huang and Reichardt, 2001). As a potent, highly selective, and novel TrkB antagonist, ANA-12 can cross the blood-brain barrier without compromising neuronal survival (Cazorla et al., 2011). Our *in vivo* results showed that the expression of BDNF peaked 24 hours after modeling and then decreased. On day

7 after the operation, the levels of BDNF and phosphorylated TrkB were lower in the MCAO/R group compared with the sham group. After EA, increased BDNF expression was accompanied by the upregulation of p-TrkB expression. However, the administration of ANA-12 did not alter the levels of BDNF and TrkB. BDNF and TrkB receptors are expressed in both dendrites and axons (Lv et al., 2018). Abnormal expression of BDNF and TrkB results in dysfunction in both dendrites and axons. The production of BDNF facilitates synapse formation, axon branching, dendrite pruning, and spine turnover (Sleiman et al., 2016). Dendritic spine density and the number, spatial distribution, and complexity of dendritic branches are crucial to dendritic signal integration and neuronal connectivity (Jones et al., 2014). In the current study, Sholl analysis of dendritic complexity and summaries of total dendritic length showed a rescue of normal dendritic length and complexity following EA treatment. The stable expression of synaptic proteins, such as synapsin-1 and PSD95, which may be modulated by BDNF/TrkB signaling, is associated with normal synaptic function (Lv et al., 2018). PSD95 is the most abundant postsynaptic scaffolding protein that regulates the size and shape of dendritic spines (Olivero et al., 2018), and synapsin-1 is involved in nerve signal transmission (Südhof et al., 1989). MAP-2 is a neuron-specific protein that plays an important role in stabilizing and determining dendritic shape in postmitotic neurons (Kosik and Finch, 1987). In this study, rats subjected to EA after ischemia/reperfusion injury exhibited increased expression of PSD95, synapsin-1, and MAP-2 proteins in the penumbra. Nogo-A is one of the major inhibitors of neurite outgrowth, and limits neuronal plasticity and functional recovery after CNS injury (Pradhan et al., 2010). In the present study, the expression of Nogo-A and NgR was significantly increased in the MCAO/R group compared with the sham group, whereas the levels were significantly reduced in the MCAO/R + EA group. Additionally, LFB staining showed a decrease in myelinated fibers in the MCAO/R group compared with the sham group, and this decrease was significantly larger in the MCAO/R + ANA-12 group than in the other groups. The present results show that EA treatment can promote neurogenesis and myelin repair in the ischemic penumbra via the BDNF/TrkB pathway.

Several limitations should be noted regarding this study. First, we examined the essential roles of the EA and BDNF/TrkB pathways in the regulation of synaptic structural and functional plasticity. Long-term potentiation and long-term depression were not investigated owing to the experimental conditions. Second, because of practical limitations, we analyzed only one time point: 7 days post-MCAO/R. Hence, further studies should include analyses at other time points. In conclusion, we examined whether EA could increase neuronal survival and induce dendrite regeneration, and found that it enhanced neuronal plasticity and functional recovery via the BDNF/TrkB pathway. The results of our study suggest that EA could be a safe and effective tool for promoting functional recovery after ischemic stroke.

**Acknowledgments:** The experiments were carried out with the help of the Clinical Research Institute of Integrative Medicine Affiliated to Shanghai Academy of Traditional Chinese Medicine and Shanghai Research Institute of Acupuncture and Meridian of China.

**Author contributions:** Study conception and design: SSL, XYH and MXZ; experiment implementation and statistical analysis: SSL, XXX and ZZM; manuscript draft: SSL, JJW and JM; manuscript revision: CLS and JGX. All authors read and approved the final manuscript.

**Conflicts of interest:** The authors declare that the article content was composed in the absence of any commercial or financial relationships that could be construed as a potential conflict of interest.

**Financial support:** This work was supported by the National Key R&D Program of China, No. 2018YFC2001600 (to JGX), the National Natural Science Foundation of China, No. 81902301 (to JJW), Budgetary Project of Shanghai University of Traditional Chinese Medicine of China, No. 2019LK024 (to JJW), Intelligent Medical Program of Shanghai (Municipal)

Health Commission of China, No. 2018ZHYL0216 (to CLS), Clinical Science and Technology Innovation Project of Shanghai Shen Kang Hospital Development Center of China, No. SHDC12018126 (to CLS), Accelerated the Development of Traditional Chinese Medicine Three-Year Action Plan Project (of Shanghai Health Commission) of China, Nos. ZY(2018-2020)-CCCX-2001-06 (to JGX and CLS) and ZY(2018-2020)-CCCX-2004-05 (to JGX and CL). The funding sources had no role in study conception and design, data analysis or interpretation, paper writing or deciding to submit this paper for publication.

**Institutional review board statement:** The study was approved by the Animal Care Committee of Shanghai University of Traditional Chinese Medicine (approval No. PZSHUTCM200110002).

**Copyright license agreement:** The Copyright License Agreement has been signed by all authors before publication.

**Data sharing statement:** Datasets analyzed during the current study are available from the corresponding author on reasonable request.

**Plagiarism check:** Checked twice by iThenticate.

**Peer review:** Externally peer reviewed.

**Open access statement:** This is an open access journal, and articles are distributed under the terms of the Creative Commons Attribution-NonCommercial-ShareAlike 4.0 License, which allows others to remix, tweak, and build upon the work non-commercially, as long as appropriate credit is given and the new creations are licensed under the identical terms.

## References

- Ali MHM, Rakib F, Abdelalim EM, Limbeck A, Mall R, Ullah E, Mesaeli N, McNaughton D, Ahmed T, Al-Saad K (2018) Fourier-transform infrared imaging spectroscopy and laser ablation-ICPMS new vistas for biochemical analyses of ischemic stroke in rat brain. *Front Neurosci* 12:647.
- Andres-Alonso M, Ammar MR, Butnaru I, Gomes GM, Acuña Sanhuesa G, Raman R, Yuanxiang P, Borgmeyer M, Lopez-Rojas J, Raza SA, Brice N, Hausrat TJ, Macharadze T, Diaz-Gonzalez S, Carlton M, Failla AV, Stork O, Schweizer M, Gundelfinger ED, Krussell M, et al. (2019) SIPA1L2 controls trafficking and local signaling of TrkB-containing amphisomes at presynaptic terminals. *Nat Commun* 10:5448.
- Bathina S, Das UN (2015) Brain-derived neurotrophic factor and its clinical implications. *Arch Med Sci* 11:1164-1178.
- Cazorla M, Prémont J, Mann A, Girard N, Kellendonk C, Rognan D (2011) Identification of a low-molecular weight TrkB antagonist with anxiolytic and antidepressant activity in mice. *J Clin Invest* 121:1846-1857.
- Chavez LM, Huang SS, MacDonald I, Lin JG, Lee YC, Chen YH (2017) Mechanisms of acupuncture therapy in ischemic stroke rehabilitation: a literature review of basic studies. *Int J Mol Sci* 18:2270.
- Che R, Zhao W, Ma Q, Jiang F, Wu L, Yu Z, Zhang Q, Dong K, Song H, Huang X, Ji X (2019) rt-PA with remote ischemic postconditioning for acute ischemic stroke. *Ann Clin Transl Neurol* 6:364-372.
- Cheatwood JL, Emerick AJ, Kartje GL (2008) Neuronal plasticity and functional recovery after ischemic stroke. *Top Stroke Rehabil* 15:42-50.
- Chen SQ, Cai DC, Chen JX, Yang H, Liu LS (2020) Altered brain regional homogeneity following contralateral acupuncture at Quchi (LI 11) and Zusanli (ST 36) in ischemic stroke patients with left hemiplegia: an fMRI study. *Chin J Integr Med* 26:20-25.
- Choo M, Miyazaki T, Yamazaki M, Kawamura M, Nakazawa T, Zhang J, Tanimura A, Uesaka N, Watanabe M, Sakimura K, Kano M (2017) Retrograde BDNF to TrkB signaling promotes synapse elimination in the developing cerebellum. *Nat Commun* 8:195.
- Ding H, Chen J, Su M, Lin Z, Zhan H, Yang F, Li W, Xie J, Huang Y, Liu X, Liu B, Zhou X (2020) BDNF promotes activation of astrocytes and microglia contributing to neuroinflammation and mechanical allodynia in cyclophosphamide-induced cystitis. *J Neuroinflammation* 17:19.
- Duris K, Splichal Z, Jurajda M (2018) The role of inflammatory response in stroke associated programmed cell death. *Curr Neuropharmacol* 16:1365-1374.
- Eftimiadi G, Soligo M, Manni L, Di Giuda D, Calcagni ML, Chiaretti A (2021) Topical delivery of nerve growth factor for treatment of ocular and brain disorders. *Neural Regen Res* 16:1740-1750.
- Falcicchia C, Paolone G, Emerich DF, Lovisari F, Bell WJ, Fradet T, Wahlberg LU, Simonato M (2018) Seizure-suppressant and neuroprotective effects of encapsulated BDNF-producing cells in a rat model of temporal lobe epilepsy. *Mol Ther Methods Clin Dev* 9:211-224.
- Francis JT, Song W (2011) Neuroplasticity of the sensorimotor cortex during learning. *Neural Plast* 2011:310737.
- Huang EJ, Reichardt LF (2001) Neurotrophins: roles in neuronal development and function. *Annu Rev Neurosci* 24:677-736.

- Hui KK, Liu J, Marina O, Napadow V, Haselgrove C, Kwong KK, Kennedy DN, Makris N (2005) The integrated response of the human cerebro-cerebellar and limbic systems to acupuncture stimulation at ST 36 as evidenced by fMRI. *Neuroimage* 27:479-496.
- Jones KA, Eng AG, Raval P, Srivastava DP, Penzes P (2014) Scaffold protein X11a interacts with kalirin-7 in dendrites and recruits it to Golgi outposts. *J Biol Chem* 289:35517-35529.
- Kaiser EE, West FD (2020) Large animal ischemic stroke models: replicating human stroke pathophysiology. *Neural Regen Res* 15:1377-1387.
- Khan MM, Wakade C, de Sevilla L, Brann DW (2015) Selective estrogen receptor modulators (SERMs) enhance neurogenesis and spine density following focal cerebral ischemia. *J Steroid Biochem Mol Biol* 146:38-47.
- Kosik KS, Finch EA (1987) MAP2 and tau segregate into dendritic and axonal domains after the elaboration of morphologically distinct neurites: an immunocytochemical study of cultured rat cerebrum. *J Neurosci* 7:3142-3153.
- Lam KY, Chen J, Lam CT, Wu Q, Yao P, Dong TT, Lin H, Tsim KW (2016) Asarone from acori Tatarinowii Rhizoma potentiates the nerve growth factor-induced neuronal differentiation in cultured PC12 cells: a signaling mediated by protein kinase A. *PLoS One* 11:e0163337.
- Lei H, Toosizadeh N, Schwenk M, Sherman S, Karp S, Sternberg E, Najafi B (2016) A pilot clinical trial to objectively assess the efficacy of electroacupuncture on gait in patients with Parkinson's disease using body worn sensors. *PLoS One* 11:e0155613.
- Lewin GR (1996) Neurotrophins and the specification of neuronal phenotype. *Philos Trans R Soc Lond B Biol Sci* 351:405-411.
- Li X, Guo F, Zhang Q, Huo T, Liu L, Wei H, Xiong L, Wang Q (2014) Electroacupuncture decreases cognitive impairment and promotes neurogenesis in the APP/PS1 transgenic mice. *BMC Complement Altern Med* 14:37.
- Li Z, Yang M, Lin Y, Liang S, Liu W, Chen B, Huang S, Li J, Tao J, Chen L (2021) Electroacupuncture promotes motor function and functional connectivity in rats with ischemic stroke: an animal resting-state functional magnetic resonance imaging study. *Acupunct Med* 39:146-155.
- Liu AJ, Li JH, Li HQ, Fu DL, Lu L, Bian ZX, Zheng GQ (2015) Electroacupuncture for acute ischemic stroke: a meta-analysis of randomized controlled trials. *Am J Chin Med* 43:1541-1566.
- Liu H, Shen X, Tang H, Li J, Xiang T, Yu W (2013) Using microPET imaging in quantitative verification of the acupuncture effect in ischemia stroke treatment. *Sci Rep* 3:1070.
- Liu L, Zhang Q, Li M, Wang N, Li C, Song D, Shen X, Luo L, Fan Y, Xie H, Wu Y (2021) Early post-stroke electroacupuncture promotes motor function recovery in post-ischemic rats by increasing the blood and brain iris. *Neuropsychiatr Dis Treat* 17:695-702.
- Liu RZ, Fan CX, Zhang ZL, Zhao X, Sun Y, Liu HH, Nie ZX, Pu XP (2017) Effects of DL-3-n-butylphthalide on cerebral ischemia infarction in rat model by mass spectrometry imaging. *Int J Mol Sci* 18:2451.
- Liu W, Wang X, Yang S, Huang J, Xue X, Zheng Y, Shang G, Tao J, Chen L (2016) Electroacupuncture improves motor impairment via inhibition of microglia-mediated neuroinflammation in the sensorimotor cortex after ischemic stroke. *Life Sci* 151:313-322.
- Longa EZ, Weinstein PR, Carlson S, Cummins R (1989) Reversible middle cerebral artery occlusion without craniectomy in rats. *Stroke* 20:84-91.
- Lv C, Ma Q, Han B, Li J, Geng Y, Zhang X, Wang M (2018) Long-term dl-3-n-butylphthalide treatment alleviates cognitive impairment correlate with improving synaptic plasticity in SAMP8 mice. *Front Aging Neurosci* 10:200.
- Moon SK, Whang YK, Park SU, Ko CN, Kim YS, Bae HS, Cho KH (2003) Antispastic effect of electroacupuncture and moxibustion in stroke patients. *Am J Chin Med* 31:467-474.
- Ng TKS, Ho CSH, Tam WWS, Kua EH, Ho RC (2019) Decreased serum brain-derived neurotrophic factor (BDNF) levels in patients with Alzheimer's disease (AD): a systematic review and meta-analysis. *Int J Mol Sci* 20:257.
- Olivero P, Lozano C, Sotomayor-Zárate R, Meza-Concha N, Arancibia M, Córdova C, González-Arriagada W, Ramírez-Barrantes R, Marchant I (2018) Proteostasis and mitochondrial role on psychiatric and neurodegenerative disorders: current perspectives. *Neural Plast* 2018:6798712.
- Padmanabhan P, Martínez-Mármol R, Xia D, Götz J, Meunier FA (2019) Frontotemporal dementia mutant Tau promotes aberrant Fyn nanoclustering in hippocampal dendritic spines. *Elife* 8:e45040.
- Pamenter ME, Ryu J, Hua ST, Perkins GA, Mendiola VL, Gu XQ, Ellisman MH, Haddad GG (2012) DIDS prevents ischemic membrane degradation in cultured hippocampal neurons by inhibiting matrix metalloproteinase release. *PLoS One* 7:e43995.
- Pradhan AD, Case AM, Farrer RG, Tsai SY, Cheatwood JL, Martin JL, Kartje GL (2010) Dendritic spine alterations in neocortical pyramidal neurons following postnatal neuronal Nogo-A knockdown. *Dev Neurosci* 32:313-320.
- Qin C, Liu Q, Hu ZW, Zhou LQ, Shang K, Bosco DB, Wu LJ, Tian DS, Wang W (2018) Microglial TLR4-dependent autophagy induces ischemic white matter damage via STAT1/6 pathway. *Theranostics* 8:5434-5451.
- Qin L, Jing D, Parada S, Carmel J, Ratan RR, Lee FS, Cho S (2014) An adaptive role for BDNF Val66Met polymorphism in motor recovery in chronic stroke. *J Neurosci* 34:2493-2502.
- Sakai S, Shichita T (2019) Inflammation and neural repair after ischemic brain injury. *Neurochem Int* 130:104316.
- Schmittgen TD, Livak KJ (2008) Analyzing real-time PCR data by the comparative C(T) method. *Nat Protoc* 3:1101-1108.
- Sleiman SF, Henry J, Al-Haddad R, El Hayek L, Abou Haidar E, Stringer T, Ulja D, Karuppagounder SS, Holson EB, Ratan RR, Ninan I, Chao MV (2016) Exercise promotes the expression of brain derived neurotrophic factor (BDNF) through the action of the ketone body  $\beta$ -hydroxybutyrate. *Elife* 5:e15092.
- Südhof TC, Czernik AJ, Kao HT, Takei K, Johnston PA, Horiuchi A, Kanazir SD, Wagner MA, Perin MS, De Camilli P, Greengard P (1989) Synapsins: mosaics of shared and individual domains in a family of synaptic vesicle phosphoproteins. *Science* 245:1474-1480.
- Sun G, Miao Z, Ye Y, Zhao P, Fan L, Bao Z, Tu Y, Li C, Chao H, Xu X, Ji J (2020) Curcumin alleviates neuroinflammation, enhances hippocampal neurogenesis, and improves spatial memory after traumatic brain injury. *Brain Res Bull* 162:84-93.
- Tian GH, Tao SS, Chen MT, Li YS, Li YP, Shang HC, Tang XY, Chen JX, Tang HB (2016) Electroacupuncture treatment alleviates central poststroke pain by inhibiting brain neuronal apoptosis and aberrant astrocyte activation. *Neural Plast* 2016:1437148.
- Veltkamp R, Gill D (2016) Clinical trials of immunomodulation in ischemic stroke. *Neurotherapeutics* 13:791-800.
- VonDrän MW, LaFrancois J, Padow VA, Friedman WJ, Scharfman HE, Milner TA, Hempstead BL (2014) p75<sup>NTR</sup>, but not proNGF, is upregulated following status epilepticus in mice. *ASN Neuro* 6:1759091414552185.
- Wang G, Lei C, Tian Y, Wang Y, Zhang L, Zhang R (2019) Rb1, the primary active ingredient in Panax ginseng C.A. Meyer, exerts antidepressant-like effects via the BDNF-TrkB-CREB pathway. *Front Pharmacol* 10:1034.
- Wang L, Zhang Z, Wang Y, Zhang R, Chopp M (2004) Treatment of stroke with erythropoietin enhances neurogenesis and angiogenesis and improves neurological function in rats. *Stroke* 35:1732-1737.
- Wang WJ, Zhong YB, Zhao JJ, Ren M, Zhang SC, Xu MS, Xu ST, Zhang YJ, Shan CL (2021) Transcranial pulse current stimulation improves the locomotor function in a rat model of stroke. *Neural Regen Res* 16:1229-1234.
- Waterhouse EG, Xu B (2009) New insights into the role of brain-derived neurotrophic factor in synaptic plasticity. *Mol Cell Neurosci* 42:81-89.
- Xiao LY, Wang XR, Yang Y, Yang JW, Cao Y, Ma SM, Li TR, Liu CZ (2018) Applications of acupuncture therapy in modulating plasticity of central nervous system. *Neuromodulation* 21:762-776.
- Xie Q, Cheng J, Pan G, Wu S, Hu Q, Jiang H, Wang Y, Xiong J, Pang Q, Chen X (2019) Treadmill exercise ameliorates focal cerebral ischemia/reperfusion-induced neurological deficit by promoting dendritic modification and synaptic plasticity via upregulating caveolin-1/VEGF signaling pathways. *Exp Neurol* 313:60-78.
- Xu X, Feng X, He M, Zhang Z, Wang J, Zhu H, Li T, Wang F, Sun M, Wang Z (2020) The effect of acupuncture on tumor growth and gut microbiota in mice inoculated with osteosarcoma cells. *Chin Med* 15:33.
- Zhang Y, Zhu Z, Liang HY, Zhang L, Zhou QG, Ni HY, Luo CX, Zhu DY (2018) nNOS-CAPON interaction mediates amyloid- $\beta$ -induced neurotoxicity, especially in the early stages. *Aging Cell* 17:e12754.
- Zhao L, Chen J, Liu CZ, Li Y, Cai DJ, Tang Y, Yang J, Liang FR (2012) A review of acupoint specificity research in china: status quo and prospects. *Evid Based Complement Alternat Med* 2012:543943.
- Zheng Y, Ji S, Czerwinski A, Valenzuela F, Pennington M, Liu S (2014) FITC-conjugated cyclic RGD peptides as fluorescent probes for staining integrin  $\alpha$ v $\beta$ 3/ $\alpha$ v $\beta$ 5 in tumor tissues. *Bioconj Chem* 25:1925-1941.
- Zou F, Lin YF, Chen SG, Cao L, Wang HR, Ye B, Wang Q, Jie-Ying H, Jia J (2020) The impact of electroacupuncture at Hegu, Shoushanli, and Quchi based on the theory "Treating Flaccid Paralysis by Yangming Alone" on stroke patients' EEG: a pilot study. *Evid Based Complement Alternat Med* 2020:8839491.

C-Editor: Zhao M; S-Editors: Yu J, Li CH; L-Editors: Yu J, Song LP; T-Editor: Jia Y